Landslides
DOI 10.1007/s10346-020-01415-5
Received: 31 May 2019
Accepted: 21 April 2020

P. Lollino · D. Giordan · P. Allasia · N. L. Fazio · M. Perrotti · F. Cafaro

Assessment of post-failure evolution of a large earthflow through field monitoring and numerical modelling

Abstract The analysis of the residual hazard existing after the emergency phases generated by the activation or reactivation of landslides is rarely taken into account in a proper manner. However, the assessment of landslide post-failure evolution should represent a key factor to control potential landslide reactivations and prevent new landslide-induced damages. This paper presents the results of a long-term field monitoring activity performed in the years after the emergency phase of the Montaguto (Italy) earthflow reactivation occurred in 2010 as well as the results of 2-D and 3-D numerical analyses aimed at interpreting the post-emergency landslide behaviour. The results of the numerical simulations, which agree well with the in situ monitoring data, allow to define a conceptual model of the earthflow behaviour that is related to the pore water pressure variations resulting from the drained or undrained processes occurring in the landslide body. The study proposed confirms a general reduction of the landslide activity, as well as allows to detect the factors that control the residual activity existing in a specific area of the landslide and to infer possible critical scenarios for landslide reactivations.

Keywords Near real-time monitoring · Numerical Modelling · Earthflow · Post-emergency evolution · Residual hazard

Introduction

The application of real-time or near real-time monitoring is widely considered to be the most efficient way to control the hazard associated with the unstable areas of a landslide during the most critical phases, and to support the risk management related to the landslide failure (Manconi and Giordan 2016). Monitoring networks generally provide an efficient support to manage an early-warning system for public safety or risk management purposes (e.g. Crosta et al. 2015; Giordan et al. 2019; Intrieri et al. 2019). However, a more comprehensive understanding of the landslide behaviour and the kinematical evolution, as well as of the corresponding controlling factors, can be more reliable when supported by the results of the application of numerical modelling techniques. As such, modelling can provide a physically or mechanically based conceptual and interpretative model of the landslide process, to be calibrated by means of the same field monitoring data (Picarelli et al. 2005; Cotecchia et al. 2015; Lollino et al. 2016). In particular, detailed studies concerning the interpretation of flow landslide mechanisms, based on both the available monitoring dataset and the results of numerical modelling, have been proposed by Picarelli et al. (2005, 2008), Tacher et al. (2005), Schulz et al. (2009), Conte et al. (2014), Bernardie et al. (2015) or, for the case of slow deep-seated sliding mechanisms, by Corominas et al. (2005), Crosta et al. (2014), Fernandez-Merodo et al. (2014), Lollino et al. (2016), Bru et al. (2018). As regards large slope instabilities, the evolution of the main critical phases can be very complex and last for long time periods, during which remedial works can be implemented in order to mitigate hazard. In these cases, the stabilization interventions can be progressively adjusted and improved also on the basis of the in situ monitoring results progressively achieved, according to the well-known "observational method" (Peck 1969), as described in Giordan et al. (2013), Crosta et al. (2014, 2015, 2017) and Ferrigno et al. (2015). The design of the remedial works can be planned according to a step-by-step procedure, so that the results of a phase of monitoring activity of the landslide evolution and of the efficacy of mitigation interventions already implemented in the slope should be used to plan the subsequent remedial works and management actions (Popescu 1996).

Following this approach, special attention should be paid to the so-called *post-failure stage*, i.e. the stage that follows the slope failure (Leroueil 2001), or in general to the *post-emergency stage*, that is the stage following the emergency phase. Indeed, in these stages the need to investigate both the landslide evolution and the residual hazard cannot be ignored for the aims of civil protection and landslide risk management.

The comprehension and the correct management of the post-failure stage is an important aspect in particular in landslides that are characterized by a long and complex evolution like large earthflows. In last decade, several papers have studied mechanisms and factors that control the evolution of earthflows focusing on: geological and geomorphological observations (Guerriero et al. 2013; Pinto et al. 2016) and field monitoring activity (Picarelli et al. 2005; Schulz et al. 2009; Giordan et al. 2013) as well as numerical modelling (Comegna et al. 2007; Lollino et al. 2017). In particular, Pellegrino et al. (2000), Picarelli et al. (2005) and Comegna et al. (2007) have explained the different stages characterizing an earthflow process, starting from the initial undrained and flow-type stage, characterized by intensive landslide activity and high movement rates, to the final drained stages, when the landslide hydraulic regime is more in equilibrium with the boundary conditions. In the final stage, the landslide mechanism takes place mainly as a sliding process and the landslide movements are significantly reduced. The role of excess pore water pressures in the regulation of the kinematics of earthflows and flow landslides has been also discussed in the past by Van Asch et al. (2007), who mention the role of rapid changes in total stresses and consequent changes in pore pressure under undrained conditions in the control of the La Valette landslide mobility, and Iverson et al. (2015), who discuss the role of liquefaction of saturated sediments at the base of the Oso landslide in the high landslide mobility.

In the present paper, we focus specifically on the analysis of the post-failure evolution of a large active earthflow, the Montaguto earthflow (Campania region, Southern Italy; Fig. 1 a and b), in the

Published online: 02 May 2020

period between the end of 2010 and the beginning of 2019. The 2010–2019 period corresponds to the phase that has followed the most critical landslide event which occurred in spring 2010. The Montaguto landslide is one of the larger active earthflow throughout Europe (Bellanova et al. 2018) and caused significant emergencies both in 2006 and in 2010, when important reactivations gave rise to the interruption of a national road and the Naples-Bari railway located at the toe of the slope (Giordan et al. 2013).

We also present a possible framework for the interpretation of the recent evolution of the Montaguto earthflow case study and the analysis of the factors that have controlled the landslide post-failure phase. The framework has been developed taking into account (i) the results of a prolonged monitoring activity based on near real-time topographic RTS (robotized total station) data, (ii) the inclinometric measurements and continuous piezometer data acquired throughout the earthflow channel and (iii) the outcomes of 2-D and 3-D finite element analyses of the landslide evolution. Starting from the outcomes of the monitoring activity and the numerical study, in the following sections, we also present some indications in terms of residual hazard associated with the earthflow activity as well as possible future scenarios of landslide evolution. The Montaguto landslide is characterized by a long and complex history described by Giordan et al. (2013), Guerriero et al. (2013) and Lollino et al. (2014). This long history is characterized by two recent main activations occurred in 2004–2006 and 2010, when the landslide toe reached the bottom of the valley and interrupted firstly the national road and then the railway. The interruption of the railway caused a severe emergency condition and the activation of the Italian National Civil Protection Department supported a multidisciplinary emergency team (Ferrigno et al., 2017). The monitoring network was installed soon after the second reactivation event occurred in 2010, and has been used to manage the corresponding emergency stage, improve the knowledge of the specific landslide phenomenon and control the efficacy of the remedial works implemented in 2011–2012 for risk mitigation. Later on, the monitoring network was reduced and the main purpose was re-addressed to the control of the less stable sectors located in the central part of the landslide. This work is also aimed at remarking how the use of a complex monitoring network can be used to calibrate a numerical model aimed at interpreting the past kinematical evolution of the landslide and, later on, to derive the effects of possible future evolution scenarios.

Case study: the Montaguto landslide

The Montaguto landslide is considered one of the largest active earthflows in Europe (Bellanova et al. 2018), with an estimated mass of 6 million m^3 and a total length of about 3 km, from the scarp to the tip (Giordan et al. 2013). In 2010, a significant reactivation interrupted the national railway between Naples and Bari and the national route SS90, so that both these infrastructures were buried under a large volume of landslide debris spreading at the landslide toe (Giordan et al. 2013). Figure 1c shows an aerial photo of the Montaguto earthflow landslide and reveals the existence of a source area represented by a sliding process, a run-out channelized flow area and an accumulation area interacting with the transportation lines at the toe (Lollino et al. 2014). Between 2011 and 2013, a complex risk mitigation intervention was designed and implemented. The remediation works mainly consisted of drainage trenches developing throughout the landslide mass and umbrella-shaped anchored retaining structures filled of high-strength granular materials at the landslide tip, respectively aimed at (i) reducing the pore water pressures within the landslide mass and (ii) stabilizing the landslide toe, thus protecting the transportation lines from possible reactivations.

The landslide here examined is located on the south-facing slope of La Montagna mountain, located to the west of the Montaguto village (southern Appenines). The unstable area develops from an elevation of about 830 m a.s.l., which corresponds to the crown of the source area, to an elevation of 415 m a.s.l., within the Biferno river valley, where the landslide tip is located. The geological units outcropping in this area belong to the Miocene pelagic deposit of the Daunia unit and of the late-Messinian to early Pliocene Villamaina Formation. In the source area, from 650 m a.s.l upslope, the Faeto Flysch formation crops out, whereas the Villamaina formation crops out in the middle and lower sector of the slope (Fig. 1d). The two units are divided by a geological unconformity and the geological structure is complicated by the Miocene-Pliocene compressive tectonism followed by Quaternary tensile stress (for more details, see Guerriero et al. (2014) and therein references). According to the cross section presented in Fig. 1d, the thickness of the landslides varies from few meters in the upper part of the channel area to more than 40 m in the landslide toe (Giordan et al. 2013). The thickness of the landslide has been estimated using a DEM of differences by Giordan et al. (2013), directly measured inside the boreholes drilled in the period 2012–2013, and described by Bellanova et al. (2018) according to electric tomography surveys executed in the channel area. Figure 2 shows a schematic timeline of the main events since 2004, indicating the two major emergency stages occurred in 2006 and 2010, along with the monitoring activities carried out since 2010 on the landslide. A near real-time monitoring network, formed of ground surface displacement targets controlled by three robotized total stations (RTS), was installed in 2010 in order to investigate the landslide evolution from a topographic point of view, during the emergency and post-emergency stages (Fig. 1c). This topographic monitoring was also supplemented by a ground-based synthetic aperture radar system (Ferrigno et al. 2015). Figures 1c and 3 show the location of the topographic targets installed throughout the landslide channel. Continuous-logging vibrating-wire piezometers were installed in January 2012 along the run-out channel in order to measure the pore water pressure variations within the landslide mass (Figs. 1c and 3), whereas inclinometer tubes were installed in 2013 to derive some indications on the depth of the landslide mass (Figs. 1c and 3). Owing to the very complex mechanism of landslide evolution, the design of the remediation works was performed in accordance with the *observational method*, i.e. following a step-by-step adjustment and improvement of the interventions according to the landslide response to the stabilization works (INGE 2010; Ferrigno et al. 2015). In particular, at the beginning of remedial works design and implementation the RTS data were used to define the priority of the stabilization works, so that the intervention was initially concentrated in the upper part of the run-out channelized flow area (here named as sector A, Fig. 1c). Later on, stabilization works were extended to the rest of the channel. In this perspective, the monitoring network was gradually optimized and integrated in accordance with the progressive reduction of the displacement rate. With the evolution of stabilization works, the monitoring goal changed from the topographic

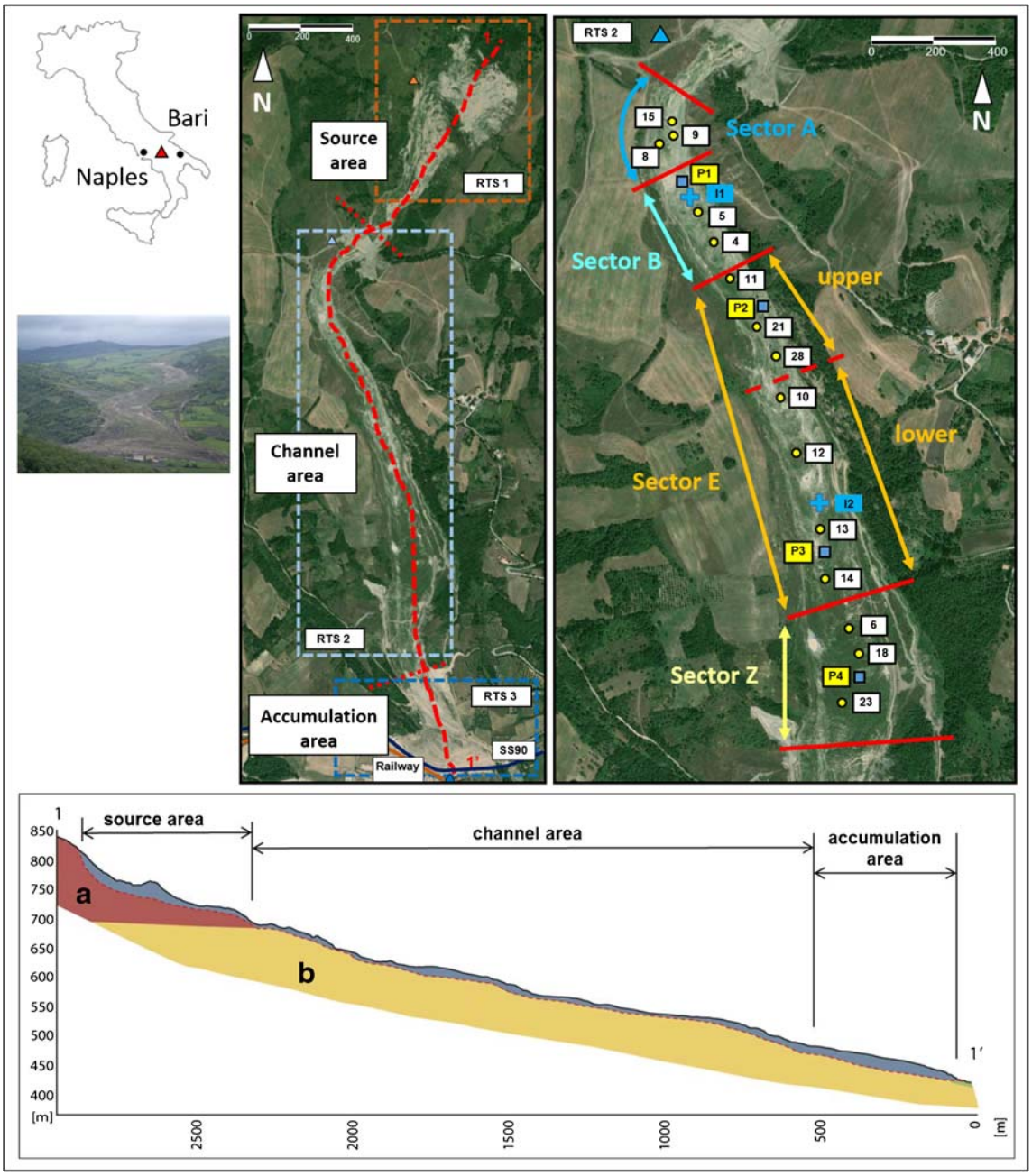

Fig. 1 **a** Location of the Montaguto landslide (red triangle). **b** Front view of the landslide (Giordan et al. 2013). **c** Aerial view of the Montaguto landslide with: the landslide areas monitored by the three robotized total stations (triangles), the indication of the landslide kinematical sectors, the national road (blue line) and the railway (brown line); the topographic targets (yellow circles), inclinometer tubes (cyan crosses) and piezometer cells (blue squares) installed along the landslide channel are also shown. **d** Geological longitudinal section of the landslide: in brown Faeto Flysch, in yellow Villamaina Unit, in grey landslide detritum (from Lollino et al. 2014)

control of the surficial landslide evolution to the three dimensional measurement of the deep landslide displacements and of the pore water pressures along the earthflow channel, which it has been the most active part of the slide in the post-failure period (Lollino et al. 2017). The channel area of the Montaguto landslide is one of the most complex sector of this gravitational process. During the study of the evolution of the landslide, we progressively defined the presence of different sectors characterized by different morphology, slope angle and kinematic behaviour. To clarify further the description of numerical model settings and results, we anticipate the definition of these sectors in this part of the manuscript and we describe the monitoring results that supported this subdivision in the following chapter. According to monitoring data acquired in the earlier post-failure stage, we divided the landslide channel in different sectors respectively named as sectors A, B, E and Z (Fig. 1c). Preliminary results concerning the monitoring activity in 2010–2011 as well as a first kinematic model of the landslide have been presented in Giordan et al. (2013) and Guerriero et al. (2013). Lollino et al. (2014) have instead remarked that in the period 1950–2006 the Montaguto earthflow has been

characterized by the alternation of phases of quiescence and landslide reactivation. This cyclic evolution results to be typical of large Italian appeninic earthflows, as well as documented by Picarelli et al. (2005) and Bertolini et al. (2005). After the 2010 failure period, the monitoring network recorded a progressive general reduction of the mobility throughout the landslide mass, but the reduction of the displacement rate was not uniform throughout the landslide. In particular, well-defined areas characterized by mobility rates larger than the rest of the earthflow mass were identified and followed with particular attention. According to Lollino et al. (2017), the activity of these sectors are related to the combination of predisposing factors as (i) the local geometry of the earthflow body, (ii) the high values of pore water pressures due to the local hydraulic regime and (iii) the development of excess pore pressures induced by undrained compression processes detected in the post-emergency phase. From this point of view, the most critical sector was identified in the central part of the landside body (sector E in Fig. 1c), and for this reason, specific attention has been paid to this part of the slope. In the following sections, the results obtained from the monitoring activity carried out between 2011 and 2019 are presented, along with numerical simulations of the landslide evolution, and the interpretation of the landslide behaviour derived for the same time span is discussed.

Monitoring observations in the post-failure phase

In the post-failure phase, during which the restoration of the infrastructures and the implementation of the drainage system in the landslide mass were carried out, higher attention was drawn to the residual activity of specific landslide sectors. In this contest, sector E was considered as one of the most critical domains of the landslide body, and for this reason, an additional monitoring system was installed to control both the ground surface movements and the deep displacements as well as the pore pressure regime in the same sector (Fig. 1c). Data acquired from the beginning of emergency condition (2010) pointed out that this was one of the most active sector. After the end of the remedial works construction, sector E continued to be the most active part of the slide and, for this reason, a most detailed analysis was carried out. More accurate data on the stratigraphic features of sector E were obtained from the boreholes drilled in the landslide mass. Field monitoring data, which cover a period of about 9 years (2010 to date), allowed to derive an interpretation of the kinematical features as well as permitted to investigate the factors responsible for the residual landslide activity. In order to investigate the pore water pressure regime within the channel area of the landslide, in January 2012 two vibrating-wire piezometer cells were installed in the channel area. In particular, P1 cell was installed in sector B, at a 7.5-m depth from g.l., and P3 cell was installed in the middle of sector E, at a 5.5-m depth (Figs. 1c and 3). P1 cell stopped working after 6 months from the installation, whereas P3 has worked up to date, thus collecting pore water pressure data for more than 7 years. Later on, in November 2013, a new piezometer cell was installed close to P1 at the same depth (named as P1n in Fig. 7), in order to continue the observations started with P1 cell. In the same period, two more piezometer cells were installed close to sector E: P2 was installed between sector B and sector E ($z = 7.5$ m from g.l.) and P4 was installed in sector Z, at 18-m depth (Figs. 1c and 3). Moreover, two boreholes drilled in 2013 were also equipped with inclinometer casings (I1 and I2 in Figs. 1c and 3). I2 has been equipped with an automatic inclinometric column. The interpretation of the landslide behaviour, as derived from all the data acquired with the whole monitoring system above described, is discussed hereafter.

The kinematical behaviour of sectors A, B and E is presented in Fig. 4a that shows the displacement registered for three specific targets 15, 5 and 13, between 2011 and 2012. According to Fig. 1c, every sector of the channel area of the landslide is monitored by several targets; in picture 4a we decided to simplify the presentation of the available dataset presenting a single target for every sector. Target 15 (sector A) registered a significant cumulated displacement of about 3 m, between January and May 2011 (average velocity: $v = 60$ cm/month), but then tends to decelerate, reaching very low displacement rates in the first months of 2012 ($v = 0.25$ cm/month). The change of trend can be probably considered an effect of the local drainage intervention installed in the same sector in 2011 and the consequent reduction of pore water pressures in the same area. In the following years, the same sector has been characterized by low displacement rates.

Target 5 describes the behaviour of sector B, which is characterized by very low slope angles (Fig. 3). The target registered small movements in the same period, with cumulated displacement lower than 20 cm (Fig. 4).

Between 2011 and 2012, target 13 (located in the middle of sector E) is observed to move with a velocity that ranges between 15 and 20 cm/month (Fig. 4). Cumulated rainfall data acquired by means of a local meteorological station (installed near the landslide crown) are also plotted in Fig. 4 and suggest that only target 13 seems to follow a seasonal trend, with limited acceleration in winter and spring (generally between January and April) and deceleration in summer and autumn.

Figure 5 reports the plot of the horizontal displacements recorded between 2012 and 2015 by a limited number of targets located along the whole earthflow channel as a function of time. In the same figure, the pore water pressures measured by the piezometric cell P3, which is located in the middle of lower sector E, are also presented. In this period, sector E (total length = 600 ÷ 700 m; average slope inclination = 6.8°) was the only sector affected by significant movements, as indicated by the curves corresponding to the central targets (10, 13 and 21) installed in this sector. Since the beginning of 2012, the registered cumulated displacements of these targets have reached maximum values of more than 2.40 m. Figure 5 also indicates that this sector exhibited a clear acceleration during March and April 2012, due to the melting of a 40–50-cm-thick snow coverage, which is testified by a strong increment of pore water pressures measured in P3 cell in the same period. Between the end of 2012 and the beginning of 2014, an approximately constant-rate increment of displacement (average velocity equal to 40 cm/year) is observed, with slight seasonal fluctuations of the displacement rate as a function of the pore water pressure variations. The targets external to sector E, like targets 5 and 11, in the upslope area, and target 23, located downslope of sector E, are instead subjected to significantly lower displacement rates. Slightly higher displacement rates have been observed in the winter between 2012 and 2013 as well as in 2014 in the upper part of sector E, hereby named as upper sector E (see target 21 in Fig. 5), where fractures opening have been clearly observed in situ in the same period. In the period between 2012

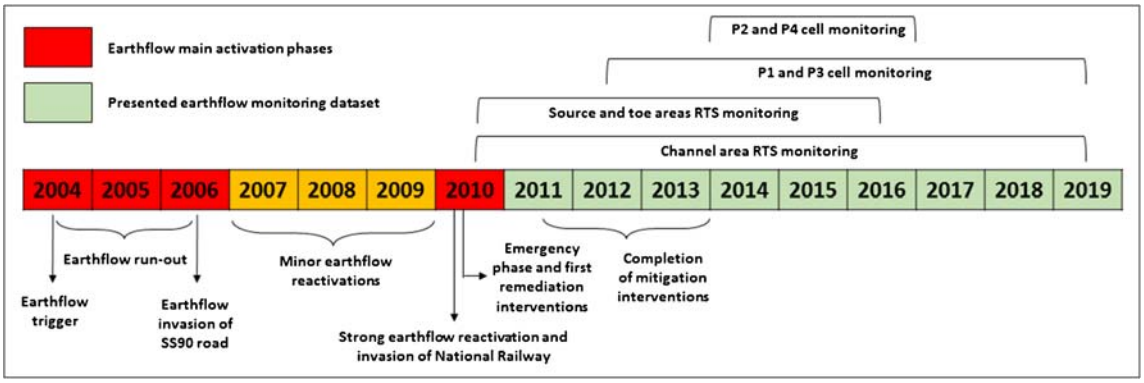

Fig. 2 Timeline of the main events and monitoring stages concerning the Montaguto reactivation processes, from 2004 to date

and 2014, the curve of pore water pressures measured by P3 piezometer cell in Fig. 5 reflects a seasonal trend with a constant average value of about 30 kPa, as described above, but a slow and continuous rising of the pore water pressures is instead observed since spring 2014. This rising of pore water pressures is supposed to be the effect of the undrained compression of the low-consolidated and low permeable detritum soils, in the area where P3 piezometer is located. This compression can be caused by the contrast of the unstable sector E against sector Z, which is practically stable (Picarelli et al. 2005; Ferrari et al. 2011; Lollino et al. 2014). The effect of the undrained compression process active in sector E on the significant rising of the piezometric heights measured in P3 cell is clearly observed in Fig. 6, where the piezometric data and the average displacement rate data measured for the central targets of sector E (10, 12, 13 and 14) are plotted against time. The figure highlights that, owing to the stability of sector Z that works as a contrast against the unstable sector E, a marked lowering of the velocity of sector E is observed between 2012 and 2019, with a reduction from 30 ÷ 35 cm/month in 2012 to less than 1 cm/month in 2019. At the same time, P3 piezometric level increases continuously, as an effect of the undrained compression mechanism of the sediments of sector E.

Figure 7 reports the piezometric data logged by the four cells in terms of the depth of piezometric level from the ground level, from the time of installation to the first months of 2019. The figure indicates that the piezometric level in P3 cell has continuously increased from 2014 to 2019, even reaching values of 16 m above the ground level that reflect the existence of high excess pore water pressures in the landslide mass as an effect of the aforementioned undrained compression of the soil debris in the same area. At present, a maximum value of the excess pore pressures has not been reached yet. P1 cell data show piezometric levels higher than

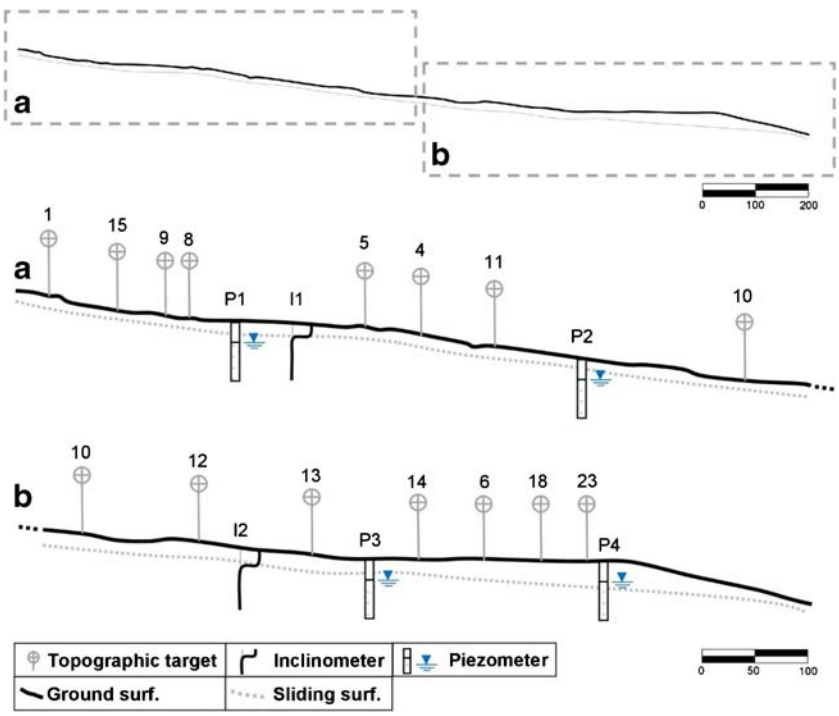

Fig. 3 Longitudinal section of the landslide channel area (Fig. 1c sectors A, B E and Z), with location of the ground surface topographic targets and boreholes equipped with inclinometers and piezometers

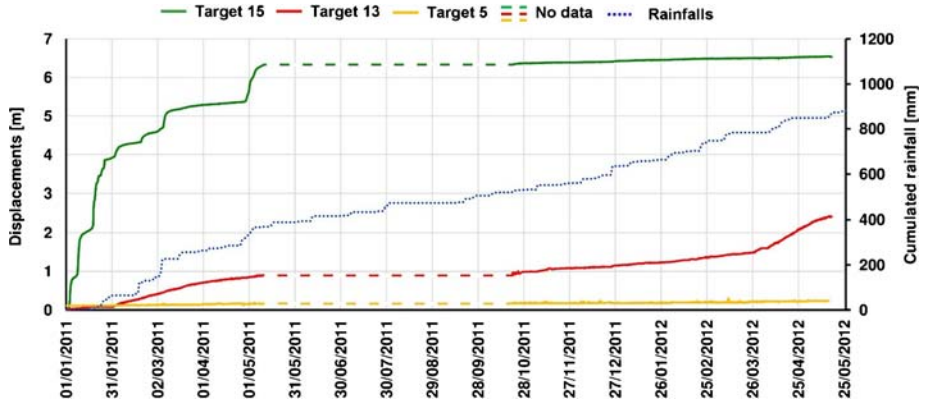

Fig. 4 Horizontal displacement for three targets along the earthflow channel and cumulated rainfall data in the period 2011–2012 (see Figs. 1c and 3 for target location)

the ground surface in the first months of 2012, rapidly decreasing as a consequence of the dissipation of excess pore water pressures, which have been presumably generated by the undrained compression of sector A against sector B in the period 2010–2011 (see Fig. 4). Since the end of 2013 (see P1n cell in Fig. 7), the piezometric level recorded in the same point seem to be more in equilibrium with the boundary conditions, thus following a seasonal trend, with an average value of about 0.8-m depth from g.l. However, since the beginning of 2015, the piezometric data seem to indicate a new slow and continuous rising, with values again higher than the ground level. Both P2 and P4 cells instead show piezometric trends that are in equilibrium with the boundary conditions (with values approximately constant with time), respectively equal to −2 m and − 10 m from the g.l.

Figure 8 a, b and c show the contours of displacement rate along the earthflow channel as defined by means of the topographic measurements respectively in the periods January 2012–June 2013, August 2013–June 2014 and July 2014–April 2015. The Kriging method has been used for the interpolation of the displacement rate data and the construction of the corresponding contours, prescribing a condition of null displacement along the landslide boundary, in accordance with the field observations. In particular, Fig. 8 a indicates that sector E was strongly active in 2012–2013, with a maximum displacement rate of about 15 cm/month in the middle-lower part. Later on, in late 2013 and 2014 (Fig. 8b), only the middle-lower portion of sector E, along with limited zones of sector B and upper sector E, remain active, with displacement rates much lower (maximum velocity $v = 4$ cm/month). Then, in late 2014 and 2015, landslide velocities further decrease (Fig. 8c).

The inclinometer profiles measured in 2013 and 2014 for I2 borehole indicate that in the same area the thickness of the landslide debris can be identified at 7–8-m depth from g.l. (Fig. 9; Lollino et al. 2017). No remarkable displacement has been instead measured from 2015 to 2018 in the upper I1 inclinometer borehole, which is located in a relatively stable area.

Except for the local process of excess pore water pressures generation above described, the data here presented prove that the remedial works, which have been implemented in 2011–2012, have generally succeeded to reduce the mobility of all the landslide sectors. At the same time, the monitoring data also highlight that the landslide phenomenon exhibits a heterogeneous behaviour throughout the whole landslide length that is generally influenced

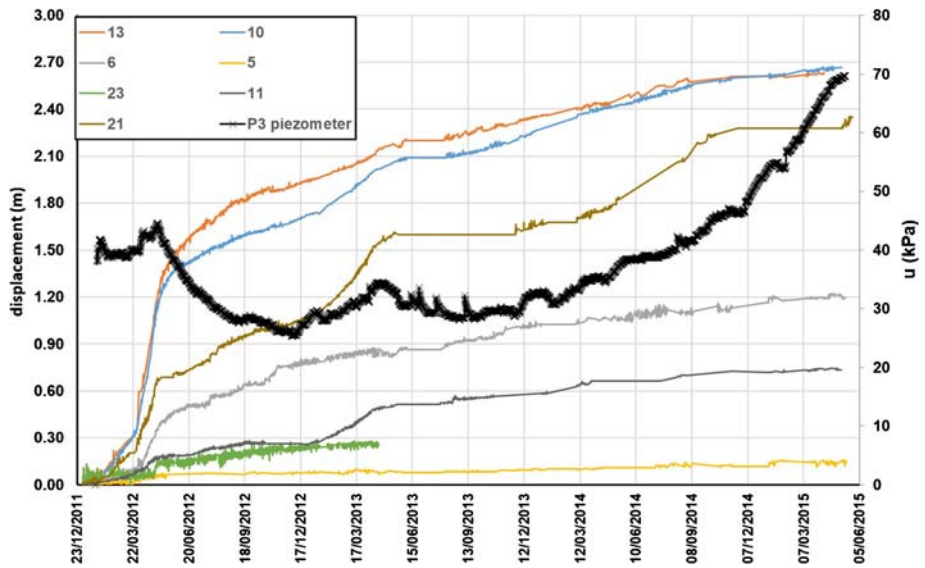

Fig. 5 Horizontal displacements and pore water pressures measured in sector E in the period 2012–2015 (see Figs. 1c and 3 for target location). Depth of installation of P3 piezometric cell, 5.5 m from g.l.

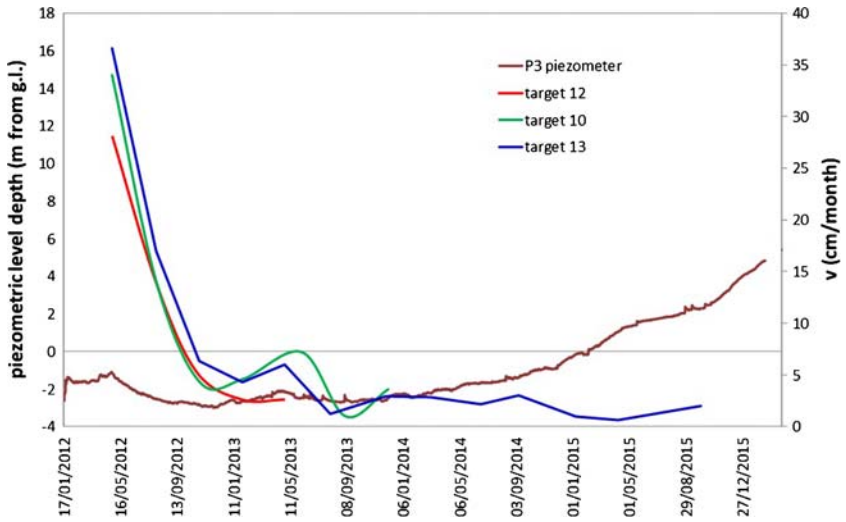

Fig. 6 Variation of average displacement rates and piezometric level depth in sector E in the period 2012–2015

by the local geometry and the hydraulic regime of the landslide mass. Such processes have been responsible for the local generation of excess pore water pressures in sector E that has not been prevented by the existing drainage system.

Numerical simulation of the landslide evolution

In this section, the application of 2- and 3-D numerical modelling techniques are proposed in order to both investigate the current stress-strain state of the landslide, which means assessing the residual hazard after the emergency phase, and explore some scenarios of possible earthflow reactivation in the future. To this purpose, the results of laboratory tests performed on debris soil samples taken from the earthflow mass are proposed in the first part in order to highlight the main features of the hydraulic and mechanical response of the material subjected to undrained loading, as well as the results of previous testing campaigns are also interpreted for modelling aims.

Material properties implemented in the simulation

The overall geotechnical behaviour of the landslide body is here supposed to mainly depend on the physical and mechanical properties of the matrix of the landslide mass debris, which derives from a deep remoulding of the original parent formation, the Faeto Flysch outcropping in the source area. The landslide deposit is matrix supported and highly heterogeneous in terms of grain size distribution and contains a good percentage of block and boulders. In order to derive the geotechnical properties of the soil matrix, two samples of the finer debris portion have been acquired and analysed. The first sample was acquired at the ground surface, while the second has been retrieved at a depth of 5.5 m from g.l.

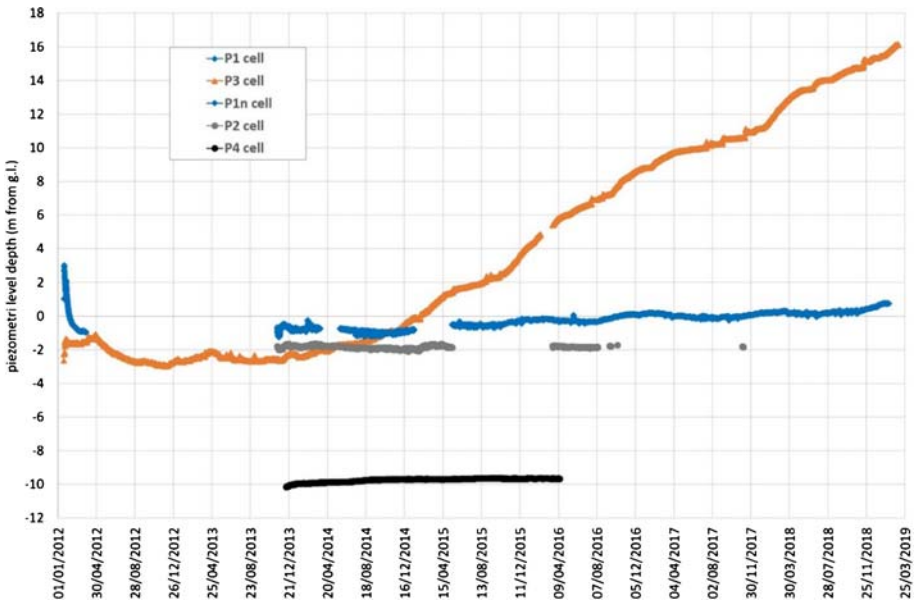

Fig. 7 Piezometric level depth from g.l. measured with four piezometer cells installed in the earthflow channel in the period 2012–2019. $P1_n$ refers to a cell which has been installed in the same position of P1; after that, P1 stopped working

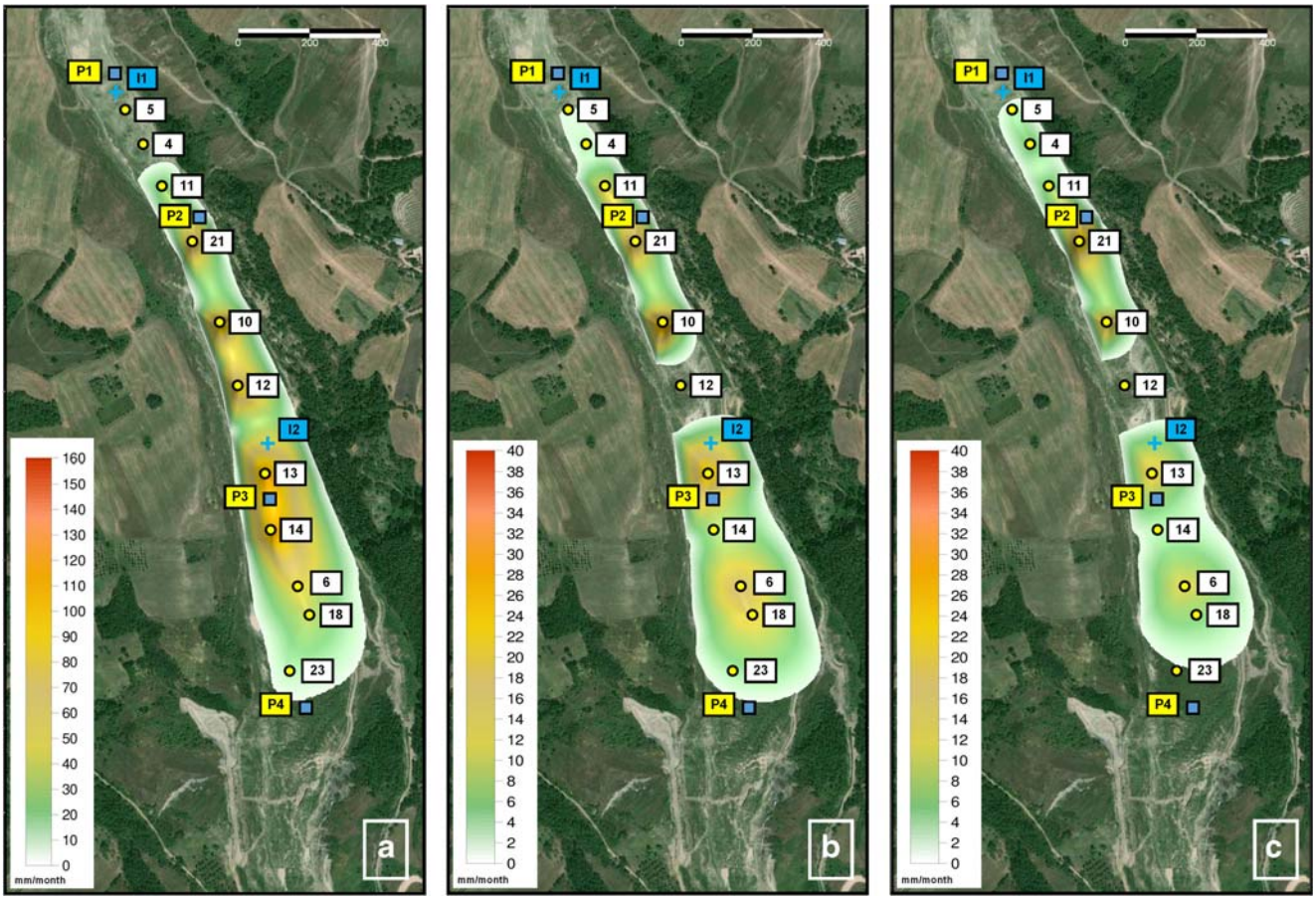

Fig. 8 Contours of average displacement rate along the channel in the time periods January 2012–June 2013 (**a**), August 2013–June 2014 (**b**), July 2014–Apr 2015 (**c**)

from the coring drilled to install P3 piezometer cell. The soil matrix can be classified as "clayey silt with sand and gravel", since the measured fine fraction is of about 70%. Atterberg limits have been determined on both samples: the liquid limit, LL, has been found to be respectively 61% and 79%, with the plasticity index, PI, equal to 20% and 29%, for the shallower and the deeper samples, respectively. Values of PI in the range 20 ÷ 45% have been indicated for the soil debris in technical reports prepared during the emergency phases. The natural water content measured on a large set of sample taken from the landslide debris ranges between 20 and 45% (Tecno-In 2006; INGE 2010). The values of the compressibility parameters c_s and c_c resulting from 1-D compression tests carried out on landslide detritum samples have been reported to be respectively in the range $c_s = 0.02–0.06$ and $c_c = 0.07–0.15$ (Tecno-In 2006; INGE 2010).

In order to investigate the mechanical behaviour of the matrix, a CIU-TRX test on a cylindrical specimen of 38-mm diameter and 76-mm height, trimmed from a sample created in the laboratory using the debris soil passing to 40 ASTM sieve of the natural sample taken at 5.5-m depth, has been carried out. To prepare the sample, the soil has been dried in the oven at 60 °C and then remoulded by adding water. The specimen has been isotropically consolidated up to a mean effective stress $p' = 110$ kPa, which is representative of a low to medium confining stress for the landslide debris. After the consolidation stage, during which the volumetric strain of the specimen has been about 1.5%, undrained shear has been applied, with rate of 0.002 mm/min. In Fig. 10, the resulting deviatoric stress–axial strain curve (a) and the excess pore water pressure–axial strain curve (b) are reported. The soil exhibits hardening-contractile behaviour, as expected for a remoulded material which did not experience important unloading. A similar behaviour has been observed for CIU triaxial tests performed on undisturbed samples retrieved from the middle-lower portion of the landslide debris mass during the 2006 investigation campaign, although with slightly larger values of excess pore water pressures generated at similar confining pressures (Tecno-In 2006).

For the investigated consolidation state, the shear modulus G at medium-strain is about 4300 kPa, and the undrained strength is $S_u = 45$ kPa (half of the deviatoric stress at failure; Fig. 10). Undrained strength values derived from several cone penetration tests carried out in the debris mass result to be on average not larger than 30–50 kPa at depths corresponding to layers classified as silty-clayey soils (Tecno-In 2006). Assuming linear strength envelope (critical state line, CSL), the test seems to indicate a critical state strength parameter M equal to 0.9 (at about $q_{cs} =$ 91 kPa and $p'_{cs} = 101$ kPa), corresponding to a friction angle of about $\phi'_{cs} = 23°$. Such a critical state strength value is consistent with that indicated in the aforementioned technical reports (Tecno-In 2006; INGE 2010) as well as with that found by Comegna and Picarelli (2008) for other similar earthslide processes in the Italian southern Apennines. It is worthwhile pointing out

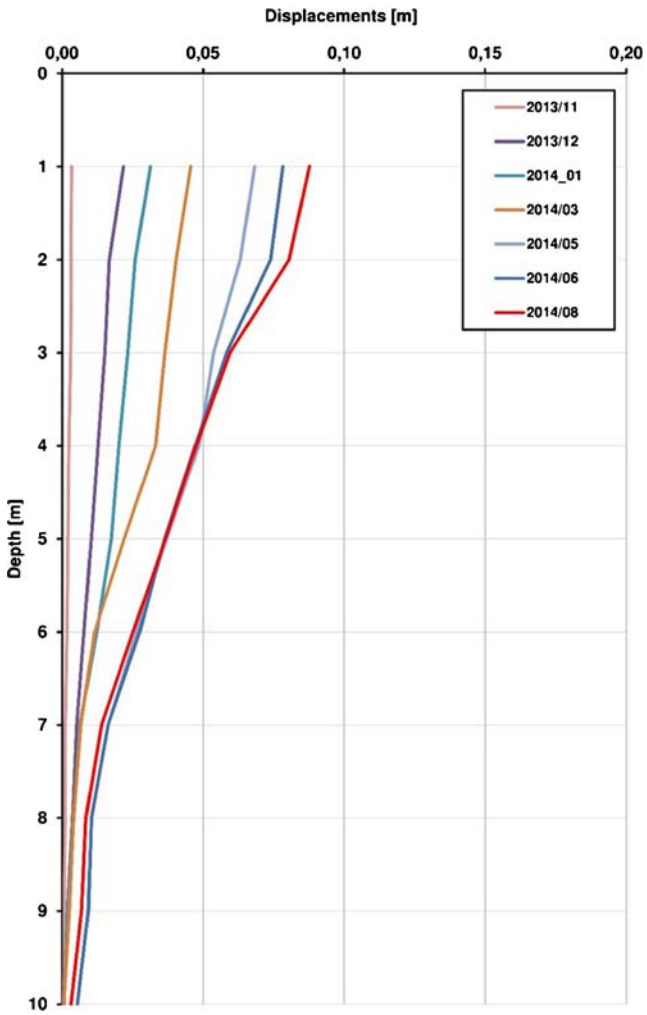

Fig. 9 Inclinometer profiles recorded at I2 casing in the period 2013–2014 (modified from Lollino et al. 2017)

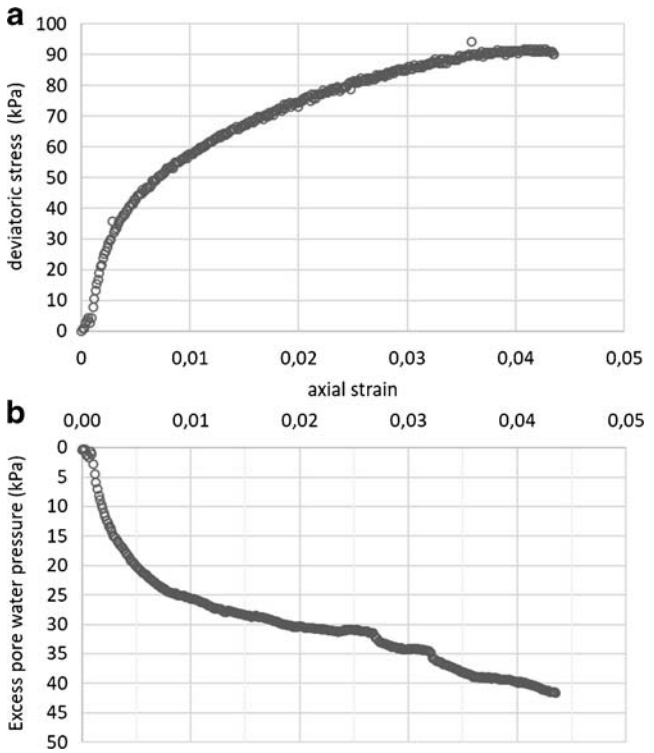

Fig. 10 Deviatoric stress vs axial strain (**a**) and excess pore water pressure vs axial strain (**b**) curves measured in consolidated-undrained triaxial compression test on a specimen trimmed from remoulded debris

that, in the landslide mass portions near the sliding surface, the friction angle of the soil matrix is supposed to be lower than 23°, approaching the residual strength, as a consequence of the large displacement sliding processes occurred in the same areas (Picarelli et al. 2008). The results of direct shear tests performed on undisturbed samples taken from the landslide debris in 2006 show a residual friction angle value equal to $\phi'_r = 19 \div 20°$ (Tecno-In 2006).

Numerical simulation of the recent landslide evolution

Following the works proposed by Picarelli et al. (2008) and Comegna et al. (2007), a 2-D short-term finite element analysis of the channel area of the landslide has been developed in order to assess the mechanism of undrained compression that is supposed to be active in sector E and to prove the development of excess pore water pressure in the area of P3 piezometer cell that follows the undrained compression of contractive soils. The model domain and the discretization mesh adopted are shown in Fig. 11a; the mesh is characterized by a minimum element size of 1 m, in the shear band area, whereas the size element in the coarser area, far from the landslide mass, reaches even 30 m. The choice of a minimum element size equal to 1 m arises from a compromise between the need of an acceptable calculation accuracy in the shear band and that of avoiding an excessive increment of the computational load that would arise from a further reduction of the element size. The domain is formed of a landslide detritum layer, overlying a 1-m-thick shear band, where shear strength is supposed to be lower than the overlying detritum soil as an effect of the large displacements occurred. The substratum underlying the shear band is considered as linear elastic, since it is supposed to be not affected by failure processes. The shear band is assumed to behave according to an elastic, perfectly plastic Mohr–Coulomb constitutive model, whereas a soft soil model with Mohr–Coulomb strength criterion, capable to simulate the undrained response of highly compressible and low-consolidated soils, has been adopted for the detritum layer. The material properties adopted for the detritum layer and the shear band have been derived from the available soil physical and mechanical characterization and are respectively summarized in Tables 1 and 2. In particular, the values of the swelling index and the compression index have been respectively derived from the compressibility parameter values described in "Material properties implemented in the simulation". The results of the undrained analysis are reported in Fig. 11 b and c, in terms of cumulated horizontal displacements and excess pore water pressures calculated at failure (when calculation stops due to the loss of convergence). In particular, Fig. 11b shows a clear unstable area that is approximately coincident with sector E, with maximum cumulated displacement larger than 1 m. The compression thrust exerted by this sector movement on the lower detritum area gives rise to excess pore water pressures in the lower area of the same sector, i.e. approximately close to P3 piezometer cell,

reaching a maximum value of 25 kPa (Fig. 11c). It is worthwhile noting that the excess pore water pressure values calculated in the analysis are approximately consistent with the values measured at failure in the triaxial test performed starting from a consolidation state representative of the piezometer depth (30–40 kPa, Fig. 10b). An increment of pore water pressures approximately equal to 30 kPa have been measured in situ with P3 piezometer cell in the period between 2013 and 2014 as a consequence of cumulated displacement of sector E equal to about 1 m (see Fig. 5). Larger cumulated displacements have been presumably occurred in situ in sector E until 2019 and excess pore water pressures even larger than 100 kPa have been then measured in P3 cell as a consequence. Therefore, the numerical results corroborate that the compression of the unconsolidated debris soils of the unstable sector E against the lower sector Z, which is stable, is capable to explain the generation of large excess pore water pressures in the area of piezometer P3.

A 3-D drained finite element analysis has been then developed with PLAXIS^{3D} software in order to investigate the stress-strain state of the landslide channel in the post-emergency phases and the factors that might explain the local residual mobility observed for sector E in the last years. In this perspective, a 3-D model is supposed to provide more accurate information than a 2-D one due to the complexity of the earthflow geometry, represented by the existence of width variations and a curved channel, and their implications in terms of mass equilibrium and stress-strain conditions. The 3-D domain has been setup by importing the digital terrain model (DTM) referred to the regional technical map dated 2011 (Fig. 12a). The numerical domain includes all the sectors A, B, E and Z of the earthflow channel and is composed of the landslide volume (plotted in green in Fig. 12a), the shear band (in dark yellow in Fig. 12a) and, all around, the rest of the volume domain. In particular, the geometry of the landslide body was reconstructed using the historical topographic mapping data, the available inclinometric data as well as the landslide mass depth data inferred from the electrical resistivity tomography survey reported in Bellanova et al. (2018). The shear band is modelled with an average thickness of 1 m and bounds the whole landslide mass. The adopted discretization mesh results from a compromise between the need of an acceptable model accuracy in the shear band and that of avoiding excessive computational loads that would arise from a further reduction of the minimum element size. In particular, the mesh is characterized by a finer element size in the earthflow volume domain, with a minimum element size of 1 m, and a maximum element size of 100 m in the coarser areas, far from the landslide mass (Fig. 12b). The boundary conditions are represented by null horizontal displacement along the vertical boundaries, whereas both horizontal and vertical displacements have been prescribed as zero at the bottom of the model. In this case, an elastic, perfectly plastic constitutive model, with a Mohr–Coulomb yield criterion, has been used for this 3-D model, for both the shear band and the landslide detritum mass. The material properties used for the shear band are those reported in Table 2; the same parameters have been assumed also for the detritum soil, except for the value of the friction angle which is consistent with the critical state value measured in the laboratory tests ($\phi' = 23°$). The rest of the domain, e.g. the stable substratum, has been instead modelled as a linear elastic material. Two different analyses implementing pore water pressure distributions consistent with the piezometric levels measured in situ respectively in 2014 and 2016 (see Fig. 6) have been implemented in the model. In particular, while in the simulation of 2014 condition the piezometric level modelled in P3 cell position has been fixed at 1 m b.g.l. (hereby, named as analysis A), in 2016 the piezometric level in the same area has been raised to 6 m above the ground level (analysis B). The modelling procedure is composed of the following stages: (1) assignment of the initial stress state by means of a gravity loading procedure; (2) plastic calculation with no shear band activated (i.e. the shear band volume has the same properties of the detritum); (3)plastic calculation with activation of the shear band (i.e. shear band friction angle reduce to the residual value).

The numerical results corresponding to analysis A are shown in Fig. 12c in terms of aerial view of the cumulated displacements, along with a longitudinal section of the earthflow. The figure clearly indicates an unstable sector, which is approximately coincident with the middle-upper area of sector E, with larger displacement values calculated in the upper part, as actually observed in situ in the same period (Fig. 7 b and c). The same results shown in terms of a longitudinal section suggest that the instability is mainly related to a local increase of the slope inclination of both the ground surface and the sliding surface, which should be combined with the high pore pressure values existing in the same landslide area, represented by piezometric levels very close to the ground surface. Moreover, the aerial view in Fig. 12c also highlights that the unstable area corresponds to a region where an increase of the landslide width occurs, thus allowing for landslide mass extension. The results obtained from analysis B (piezometric levels corresponding to 2016) are instead shown in Fig. 12d in terms of aerial view of the contours of cumulated displacements, also shown in longitudinal section. The figure highlights that, with these assumptions, a local instability (smaller than that resulting from analysis A) is observed in the middle-lower area of sector E, slightly downslope P3 piezometric cell. The rest of the landslide mass is observed to be not affected by instability processes and this is also valid for sector Z, which is deemed to be the sector controlling potential reactivations of the lower landslide area. This result seems to be consistent with the field observations gained from the monitoring displacement data, which indicate a process of downslope propagation of the instability between 2014 and 2016.

Scenario analyses of possible future landslide evolution

Finally, a scenario-based analysis has been carried out in order to predict the possible evolution of the landslide process as a consequence of significant variations of the piezometric levels with respect to the current conditions. In this case, for the sake of simplicity, 2-D analyses have been performed with the same assumptions described in the 3-D modelling described above. For these analyses, the piezometric levels assumed in P1 and P2 piezometer locations have been kept fixed to those already assumed in the 3-D analysis, which are respectively 1 m and 1.6 m below the ground level, whereas variable conditions have been assumed for P3 and P4 piezometers in order to investigate the stability of sector Z. The results corresponding to Scenario 1 (P3: $z_w = 0$ m from g.l.; P4: $z_w = 0$ from g.l.; Fig. 13a) show that the condition of water table coincident with the ground surface is not capable of triggering the instability of Sector Z, since the area corresponding to this sector is not affected by appreciable movements. Scenario 2 has instead explored the combination of

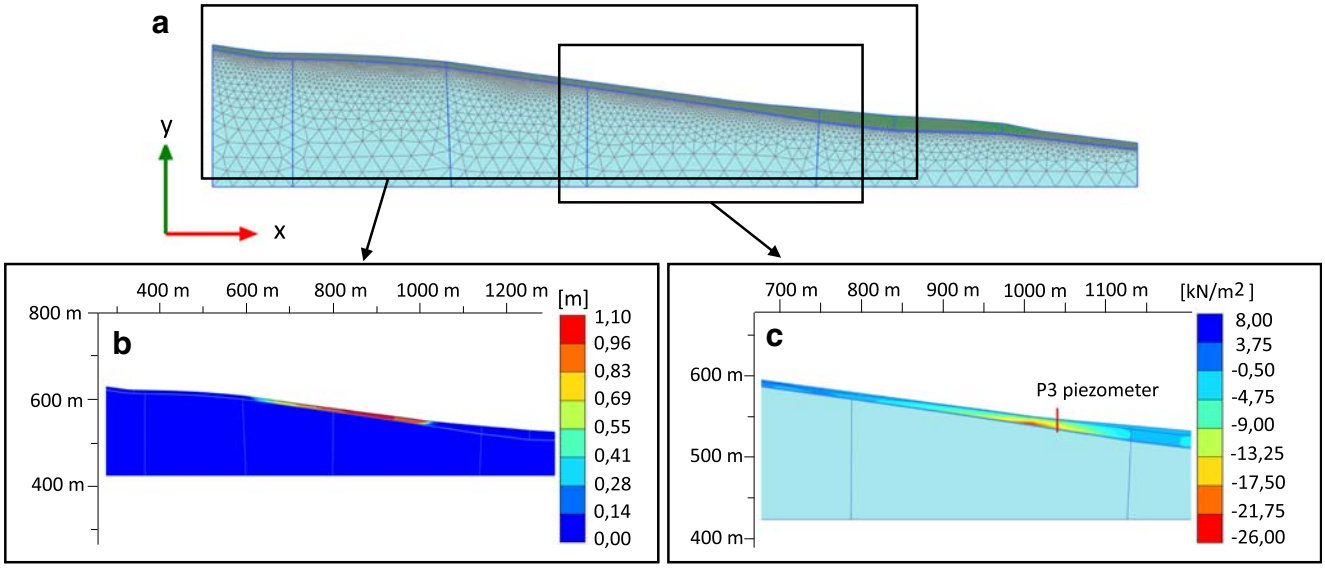

Fig. 11 2-D finite element model of sector E. **a** Discretization mesh; in dark green the detritum layer, in cyan the subsoil. **b** Calculated horizontal displacements. **c** Calculated excess pore water pressures

a piezometric level in P3 cell equal to that currently existing, while in P4 the piezometric level has been increased to the ground surface (P3: $z_w = +16$ m from g.l.; P4: $z_w = 0$ m from g.l.; Fig. 13b). Figure 13b suggests that, with a strong rise of the piezometric level in P3, as that existing at present, a piezometric level in P4 reaching the ground surface can trigger a progressive mobilization of the upper area of sector Z, although this condition should not involve the whole sector and therefore the area downslope. Further increments of the piezometric level in P4 cell, up to +10 m above the ground surface (Scenario 3; P3: $z_w = 0$ m from g.l.; P4: $z_w = +10$ m from g.l.), as for example those resulting from undrained loading processes involving the same area, can instead completely mobilize the whole sector Z (Fig. 13c). This possible evolution is also confirmed with piezometric levels assumed in P3 cell well above the ground surface, as for example in Fig. 13d, where the piezometric level is at 16 m above the ground surface (Scenario 4). These results suggest that the piezometric conditions in sector Z play a remarkable role in the stability of the middle-lower portion of the earthflow channel, irrespective of the piezometric conditions in sector E. As a matter of fact, the emergency conditions occurred in 2006 and 2010 presumably took place as a consequence of a strong rise of the piezometric levels in sector Z due to undrained loading processes produced by the thrust or the overriding of earthflow masses coming from the upper part of the channel.

Discussion and concluding remarks

In this paper, the behaviour of the Montaguto earthflow in the post-failure phase, as resulting from a large monitoring dataset acquired in several years and from the results of numerical analyses, has been presented and discussed. The availability of a long real-time and continuous monitoring time series (2010–2019) is not so common for earthflows and the corresponding dataset provides a clear framework to investigate the evolution of the Montaguto earthflow during the post-failure phase and, in general, to have an insight in the complex behaviour of earthflows and the associated hazard conditions. In this paper, we have specifically focused our attention on the long-term monitoring of Sector E, the last active sector of the landslide, along with the rest of the earthflow channel, from 2012 to date. Although the efficacy of the drainage interventions has been testified by the general reduction of the slope activity, characterized by movement rates of one order of magnitude lower than those measured during the critical phase, sector E is observed to be still unstable, with average velocity approximately equal to 40–50 cm/year that tends to reduce in the last years. The continuous monitoring of displacement and pore pressure parameters for sector E provided a clear indication of higher displacement rates in the spring season due to increment of pore water pressures measured at the depth of the shear band. A clear tendency of the failure process to retrogress has been also observed in the upper part of sector E, probably as a consequence of the stress unloading generated by the previous movement of the central portion of the sector. At present, the lowest sector of the channel area, i.e. sector Z, which is characterized by a sub-horizontal shear band and ground profile, is providing a passive thrust against the instability of sector E and, in combination with the effect of the drainage interventions, has

Table 1 Material parameters adopted for the landslide detritum in the 2-D FE model (soft soil model)

Parameter	γ (kN/m^3)	λ	κ	K_0^{NC}	c′ (kPa)	φ′ (°)	ψ (°)
Detritum soil	18	0.03	0.01	0.5	0.1	23	0

Table 2 Material parameters adopted for the shear band in the 2-D and 3-D FE model (Mohr–Coulomb model)

Parameter	γ (kN/m^3)	E′ (MPa)	ν	c′ (kPa)	φ′ (°)	ψ (°)
Shear band	18	20	0.25	0	13	0

presumably produced the slowing of the upper sectors in the last years. The undrained compression of the unstable sector E against sector Z is also giving rise to a significant increment of the pore water pressures, which at present is observed only in a limited area, the lower area of sector E. This process requires to be monitored in the future in order to check possible extensions of the area affected and, eventually, movement reactivations.

In order to improve the comprehension of the kinematics that has characterized the Sector E in the last years, numerical models consistent with the information derived from the investigations performed during the post-failure phase have been proposed and discussed. The results of the numerical simulations, which agree well with the in situ monitoring data, allow to define a conceptual model of the earthflow behaviour that is related to the pore water pressure variations resulting from the drained or undrained processes occurring in the landslide body. They also indicate the role of the geometry of the sliding surface in sector E as a factor promoting the instability of this specific area. The model has been capable to simulate the size of the unstable area and the distribution of the displacement field along sector E, in accordance with the RTS monitoring data. The role of sector Z as a passive thrust with respect to the instability of the upper sectors is also confirmed by the numerical results.

Possible future scenarios of landslide evolution have been also inferred in accordance with the results of the numerical models. Despite the general tendency to the reduction of the slope movements observed in the last years, the increase of pore water pressures in sector E suggests how, locally, the remedial works were not able to prevent the generation of excess pore

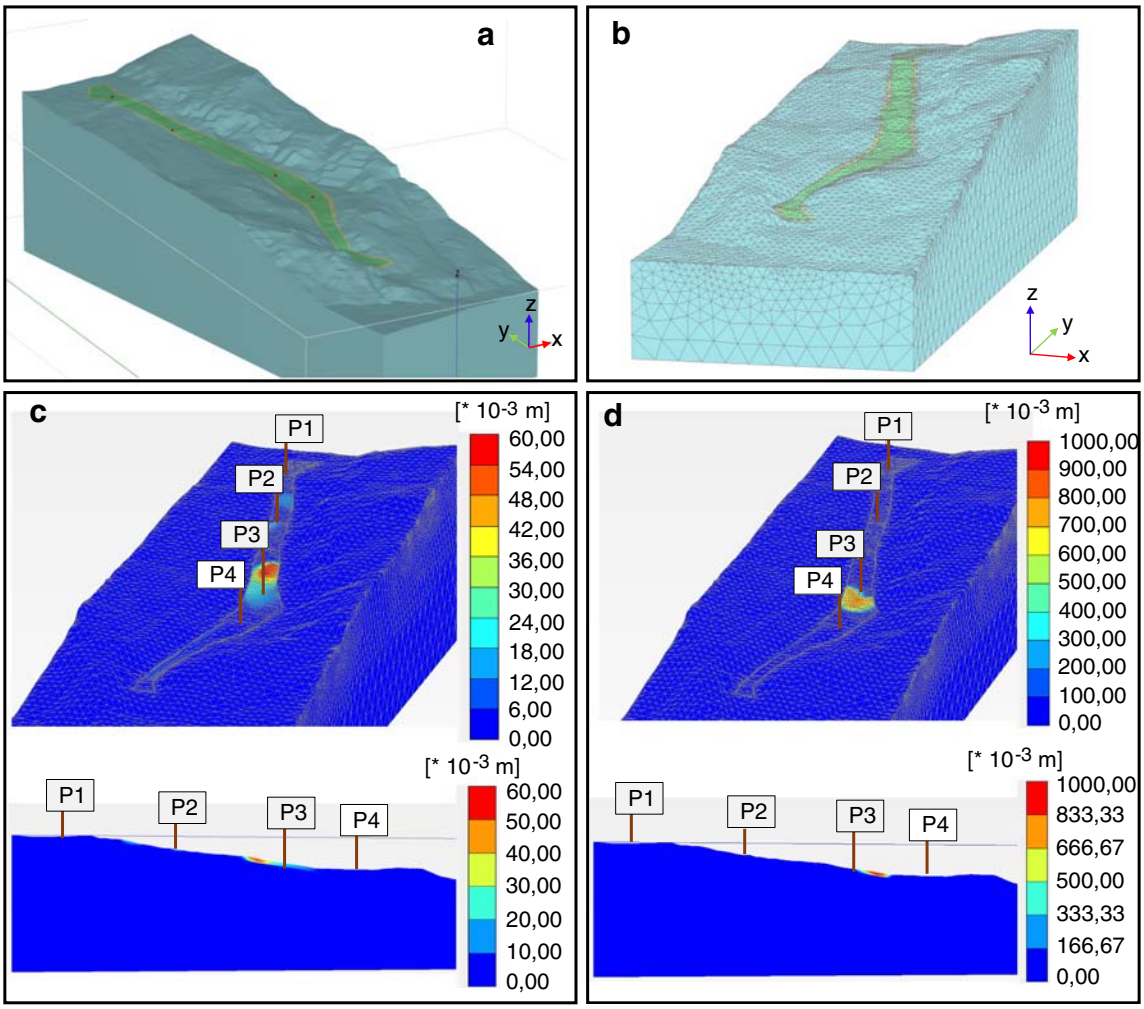

Fig. 12 3-D finite element model of the Montaguto landslide. **a** Model domain: in green the earthflow mass, in dark yellow the shear band. **b** Discretization mesh. **c** Analysis representative of the earthflow conditions in 2014: cumulated displacements. **d** Analysis representative of the earthflow conditions in 2016: cumulated displacements

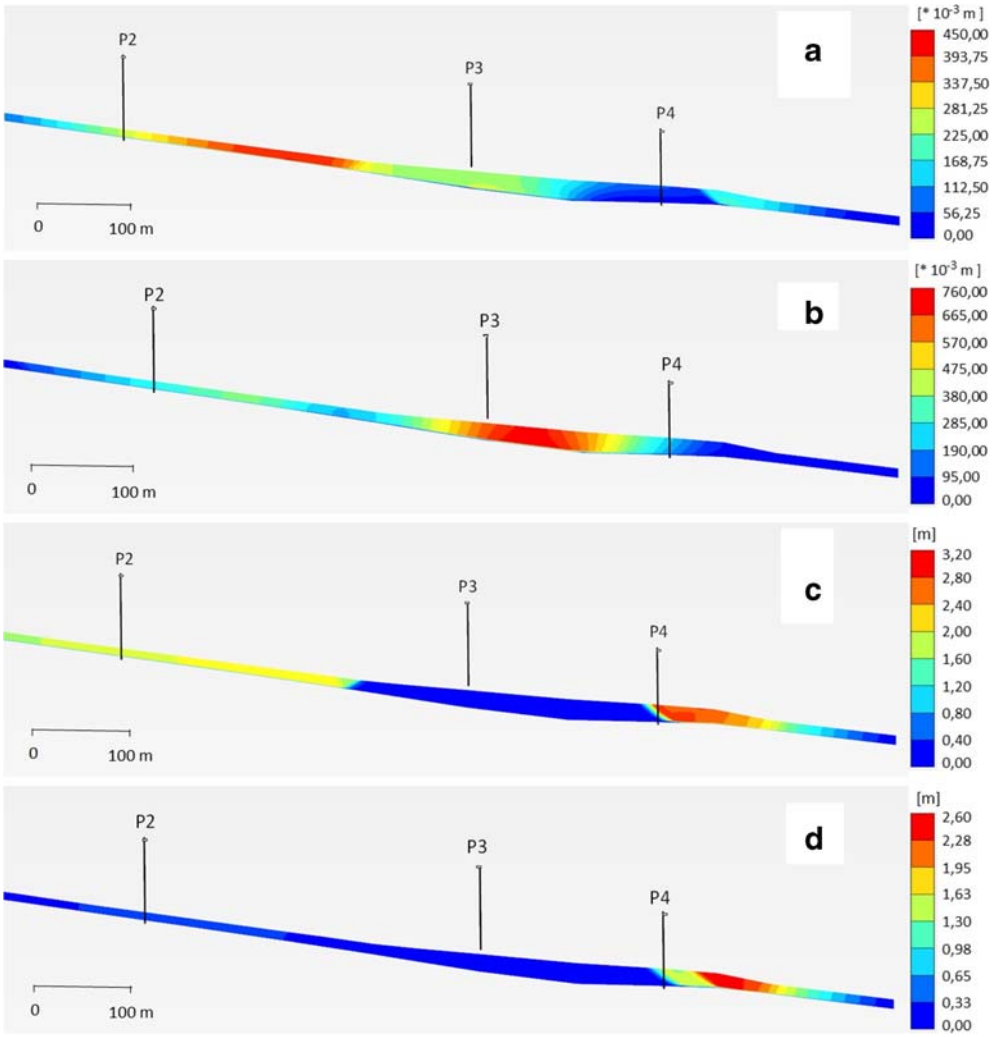

Fig. 13 Contours of the cumulated displacements calculated in scenario 1 simulation (**a**), scenario 2 (**b**), scenario 3 (**c**) and scenario 4 (**d**)

water pressures in the channel area as a consequence of undrained processes. The registered trend of pore pressures cannot be underestimated and the scenarios simulated show possible slope evolution conditions that could become critical for the stability of the whole slope. In particular, the eventual increment of pore pressures in Sector Z, with piezometric heads higher than ground level, seems to be a crucial scenario since it can give rise to the reactivation and the general destabilization of the middle and lower portion of the slope. As such, a stronger effort should be performed to focus specifically on this research theme, and in this perspective, more accurate monitoring activity and numerical modelling should be integrated in order to identify possible thresholds for the general reactivation of the lower portion of the landslide.

Acknowledgements

The emergency phase has been coordinated by the Italian Civil Protection Department, in collaboration with CNR-IRPI, University of Florence – Department of Earth Science, University of Sannio – Department of Science and Technology, and INGEO srl.

References

Bellanova J, Calamita G, Giocoli A, Luongo R, Macchiato M, Perrone A, Uhlemann S, Piscitelli S (2018) Electrical resistivity imaging for the characterization of the Montaguto landslide (southern Italy). Eng Geol 243:272–281

Bernardie S, Desramaut N, Malet JP, Gourlay M, Grandjean G (2015) Prediction of changes in landslide rates induced by rainfall. Landslides 12:481–494
Bertolini G, Guida M, Pizziolo M (2005) Landslides in Emilia-Romagna region (Italy): strategies for hazard assessment and risk management. Landslides 2(4):302–312
Bru G, Fernandez-Merodo JA, Garcia-Davalillo JC, Herrera G, Fernandez J (2018) Site scale modeling of slow-moving landslides, a 3D viscoplastic finite element modeling approach. Landslides 15:257–272
Comegna L, Picarelli L (2008) Anisotropy of a shear zone. Géotechnique 58(9):737–742
Comegna L, Picarelli L, Urciuoli G (2007) The mechanics of mudslides as a cyclic undrained-drained process. Landslides 4:217–232
Conte E, Donato A, Troncone A (2014) A finite element approach for the analysis of active slow-moving landslides. Landslides 11:723–731
Corominas J, Moya J, Ledesma A, Lloret A, Gili JA (2005) Prediction of ground displacements and velocities from groundwater level changes at the Vallcebre landslide (East-Ern Pyrenees, Spain). Landslides 2:83–96
Cotecchia F, Vitone C, Santaloia F, Pedone G, Bottiglieri O (2015) Slope instability processes in intensely fissured clays: case histories in the southern Apennines. Landslides 12:877–893
Crosta G, Di Prisco C, Frattini P, Frigerio G, Castellanza R, Agliardi F (2014) Chasing a complete understanding of the triggering mechanisms of a large rapidly evolving rockslide. Landslides 11(5):747–764
Crosta G., Lollino G., Frattini P., Giordan D., Tamburini A., Rivolta C., Bertolo D. (2015). Rockslide monitoring through multi-temporal LiDAR DEM and TLS data analysis. In: Lollino G., Giordan D., Crosta G. B., Corominas J., Azzam R., Wasowski J., Sciarra N. (eds.) Engineering geology for society and territory 2, Springer International Publishing Cham, 613–617
Crosta G, Agliardi F, Rivolta C, Alberti S, Dei CL (2017) Long-term evolution and early warning strategies for complex rockslides by real-time monitoring. Landslides 14(5):1615–1632
Fernandez-Merodo JA, Garcìa-Davalillo JC, Herrera G, Mira P, Pastor M (2014) 2D viscoplasti finite element modelling of slow landslides: the Portalet case study (Spain). Landslides 11:29–42
Ferrari A, Ledesma A, Gonzales DA, Corominas J (2011) Effects of the foot evolution on the behaviour of slow-moving landslides. Eng Geol 117:217–228
Ferrigno F, Gigli G, Fanti R, Casagli N (2015) GB-InSAR monitoring and observational method for landslide emergency management: the Montaguto earthflow (AV, Italy). Nat Hazards Earth Syst Sci Discuss 3:7247–7273
Giordan D, Allasia P, Manconi A, Baldo M, Santangelo M, Cardinali M, Corazza A, Albanese V, Lollino G, Guzzetti F (2013) Morphological and kinematic evolution of a large earthflow; the Montaguto landslide, southern Italy. Geomorphology 187:61–79
Giordan D, Wrzesniak A, Allasia P (2019) The importance of a dedicated monitoring solution and communication strategy for an effective management of complex active landslides in urbanized areas. Sustainability 11(4):946
Guerriero L, Revellino P, Coe JA, Focareta M, Grelle G, Albanese V, Corazza A, Guadagno FM (2013) Multi-temporal maps of the Montaguto earth flow in southern Italy from 1954 to 2010. J Maps 9(1):135–145
Guerriero L, Coe JA, Revellino P, Grelle G, Pinto F, Guadagno FM (2014) Influence of slip-surface geometry on earth-flow deformation, Montaguto earth flow, southern Italy. Geomorphology 219:285–305
INGE (2010). Internal technical report for the Montaguto emergency phase
Intrieri E, Carlà T, Gigli G (2019) Forecasting the time of failure of landslides at slope-scale: a literature review. Earth Sci Rev 193:333–349
Iverson RM, George DL, Allstadt K, Reid ME, Collins BD, Vallance JW, Schilling SP, Godt JW, Cannon CM, Magirl CS, Baum RL, Coe JA, Schulz WA, Bower JB (2015) Landslide mobility and hazards: implications of the 2014 Oso disaster. Earth Planet Sci Lett 412:197–208
Leroueil S (2001) Natural slopes and cuts: movement and failure mechanisms. **Géotechnique** 51:197–243
Lollino P, Giordan D, Allasia P (2014) The Montaguto earthflow: a back-analysis of the process of landslide propagation. Eng Geol 170:66–79
Lollino P, Cotecchia F, Elia G, Mitaritonna G, Santaloia F (2016) Interpretation of landslide mechanisms based on numerical modelling: two case histories. European Journal of Civil and Environmental Engineering 20(9):1032–1053. https://doi.org/10.1080/19648189.2014.985851
Lollino P, Giordan D, Allasia P (2017) Assessment of the behaviour of an active earth-slide by means of calibration between numerical analysis and field monitoring. Bull Eng Geol Environ 76(2):421–435
Manconi A, Giordan D (2016) Landslide failure forecast in near-real-time. Geomatics, Natural Hazards and Risks 7(2):639–648
Peck RB (1969) Advantages and limitations of the observational method in applied soil mechanics. Geotéchnique 19(2):171–187
Pellegrino A, Ramondini M, Russo C, Urciuoli G (2000) Kinematic features of earthflows in Southern Apeninnes. In: Bromhead EN, Dixon N, Ibsen ML (eds) Proc. 8th Int. Symp. Landslides, Cardiff (UK). Thomas Telford, London, pp 1195–2002
Picarelli L, Urciuoli G, Ramondini M, Comegna L (2005) Main features of mudslides in tectonised highly fissured clay shales. Landslides 2:15–30
Picarelli L, Olivares L, Damiano CL, E. (2008) Mechanical aspects of flow-like movements in granular and fine grained soils. Rock Mech Rock Engng 41(1):179–197
Pinto F, Guerriero L, Revellino P, Grelle G, Senatore MR, Guadagno FM (2016) Structural and lithostratigraphic controls of earth-flow evolution, Montaguto earth flow, southern Italy. J Geol Soc 173(4):649–665
Popescu ME (1996). From landslide causes to landslide remediation. Special lecture. In: Proc. 7th Int Symp on landslides, Trondheim, 1, 97–114
Schulz WH, McKenna JP, Kibler JD, Biavati G (2009) Relations between hydrology and velocity of a continuous moving landslide - evidence of pore-pressure feedback regulating landslide motion? Landslides 6:181–190
Tacher L, Bonnard C, Laloiu L, Parriaux A (2005) Modelling the behaviour of a large landslide with respect to hydrogeological and geomechanical parameter heterogeneity. Landslides 2:3–14
Tecno-In (2006). Internal technical report for the Montaguto emergency phase
Van Asch TWJ, Van Beek LPH, Bogaard TA (2007) Problems in predicting the mobility of slow-moving landslides. Eng Geol 91:46–55

P. Lollino · N. L. Fazio · M. Perrotti
CNR IRPI – Research Institute for Geo-Hydrological Protection, Italian National Research Council,
Via Amendola 122/i, 70126, Bari, Italy

D. Giordan (✉) · P. Allasia
CNR IRPI – Research Institute for Geo-Hydrological Protection, Italian National Research Council,
Strada delle Cacce 73, 10135, Torino, Italy
Email: daniele.giordan@irpi.cnr.it

F. Cafaro
DICATECH, Politecnico di Bari,
Via Orabona 4, 70125, Bari, Italy